Received: 16 April 2021 | Revised: 16 June 2021 | Accepted: 19 June 2021

DOI: 10.1002/bit.27867

ARTICLE

BIOTECHNOLOGY AND BIOENGINEERING WILEY

Impact of freeze–thaw processes on monoclonal antibody platform process development

Dennis Weber | **Christian Sittig** | **Jürgen Hubbuch**

Section IV: Biomolecular Separation Engineering, Institute of Engineering in Life Sciences, Karlsruhe Institute of Technology (KIT), Karlsruhe, Germany

Correspondence
Jürgen Hubbuch, Section IV: Biomolecular Separation Engineering, Institute of Engineering in Life Sciences, Karlsruhe Institute of Technology (KIT), Fritz-Haber-Weg 2, 76131 Karlsruhe, Germany.
Email: juergen.hubbuch@kit.edu

Abstract

Freezing of cell culture supernatant (CCS) is a standard procedure in process development of monoclonal antibody (mAb) platform processes as up- and downstream development are usually separated. In the manufacturing process of mAb, however, freezing is avoided, which poses the question of comparability and transferability from process development to manufacturing. In this case study, mAb CCS from Chinese hamster ovary (CHO) cells is frozen and thawed in a novel active freezing device and subsequently captured by protein A chromatography. Critical quality attributes such as host cell protein (HCP) concentration and soluble mAb dimer shares have been monitored throughout the case study. Furthermore, cryo-concentration of individual proteins was investigated. The main factors that drive cryo-concentration are diffusion and natural convection. Natural convection in freezing processes was found to increase at warmer freezing temperatures and thus slower freezing, leading to higher concentration gradients from top to bottom of a freezing chamber. The freeze concentration was dependent on protein size and correlated to diffusivity, where smaller proteins are exposed to higher cryo-concentration. Our results suggest that as a result of freezing processes, large particles based on mAb and specific host cell proteins (HCPs) expressing a certain affinity to mAbs are formed that have to be removed before purification. This leads to a significant improvement in HCP reduction by the protein A step, when compared with reference samples, where twice as much HCP remained in the eluate. Furthermore, HCP and mAb dimer concentrations in protein A eluate were dependent on the freezing temperature. As a conclusion, CCS should be frozen as rapidly as possible during process development to minimize issues of transferability from process development to manufacturing.

KEYWORDS

cell culture supernatant, freezing, monoclonal antibody, platform process, process development

1 | INTRODUCTION

In the biopharmaceutical market, monoclonal antibodies (mAb) are the most important class of proteins to date. Hence, many studies with industrial interest in the improvement of the manufacturing process have been published leading to the establishment of a platform process for mAb purification (Baumann & Hubbuch, 2017). A typical manufacturing process involves three major steps: cell culture, purification, and formulation. During large-scale manufacturing, each of these steps is performed subsequently, whereas all steps are evaluated individually during process development. Additionally, the up- and downstream manufacturing parts are usually located on one manufacturing site, while filling of the drug product is often done at different locations. Therefore, the product is often frozen to reduce the risk of product loss by microbial growth, foam prevention, and mechanical stress during transportation and hold times in process development (Authelin et al., 2020; Kolhe & Badkar, 2011). However, freeze–thaw (FT) process steps come with disadvantages that might lead to protein activity loss (Bhatnagar et al., 2007) such as cryo-concentration, protein–ice surface interaction (Chang et al., 1996), and cold denaturation (Privalov, 1990). These FT stresses might lead to protein aggregation (Mahler et al., 2009) and even native aggregate particle formation, which was previously reported for mAb (Telikepalli et al., 2014). Because of the high importance to the drug industry, several studies on FT processes of mAb formulations have been performed (Hauptmann et al., 2019; Miller et al., 2013; Rayfield et al., 2017). Such freezing processes are often categorized by scale and mode of cooling. Actively cooled freezing processes involve a cooling fluid, which is in contact with the container wall, whereas containers frozen in larger freezers are referred to as passive freezing processes. Across all freezing processes, cryo- or freeze concentration occurs due to exclusion of the solutes from ice crystals. This phenomenon is also well described for different solidification processes in various areas such as alloys (Shevchenko et al., 2015). From a macroscopic view, the area of solidification at the freezing front, where crystals grow into solution, is described as a "mushy zone." As a result of freeze concentration, buoyancy-driven flows also known as "natural convection" occur in the mushy zone and the remaining liquid in large scale-processes, due to density gradients. In addition to natural convection, diffusion of solutes also leads to cryo-concentration (Butler, 2002), which can be described by Fick's law.

As pointed out initially, up- and downstream process development is often done with hold times in between and process intermediates have to be frozen to increase their shelf life. This step is avoided during the manufacturing process to minimize the risk of product degradation. Despite this major difference in process development and manufacturing, no studies have been presented yet on the transferability of data characterizing unit operations across scales, where different sample preparations (frozen vs. reference) were applied. Therefore, this study investigates the impact of an additional FT cycle before a typical protein A step using cell culture supernatant (CCS) from Chinese hamster ovary (CHO) cells with mAb. Furthermore, characterization of complex freezing processes with multiple proteins is performed to provide a better understanding of freezing processes.

2 | MATERIALS AND METHODS

2.1 | Buffer preparation

All buffers have been prepared from sodium chloride (NaCl), sodium acetate (NaAc), potassium chloride (KCl), potassium hydrogen phosphate ($KHPO_4$), sodium dihydrogen phosphate-monohydrate ($NaH_2PO_4{\cdot}H_2O$), sodium hydroxide (NaOH), and acetic acid (CH_3COOH) from Merck, di-sodium hydrogen phosphate dihydrate ($Na_2HPO_4{\cdot}2H_2O$) from Sigma-Aldrich, and 20× phosphate-buffered saline (PBS) Tween™−20 from Thermo Fisher Scientific. The buffer salts were dissolved in ultrapure water (PURELAB Ultra; ELGA LabWater, Veolia Water Technologies). After adjusting the pH of all buffers to the desired pH ±0.1 using concentrated hydrochloric acid, acetic acid, or NaOH, all buffers have been filtered using 0.2 µm filter membranes and degassed in an ultrasonic water bath.

2.2 | mAb preparation

CCS of a mAb harvest with a titer of 2 g/L from CHO cells was kindly provided by Byondis. Due to the lack of stability of CCS, handling and storage of CCS is not possible without freezing. Thus, the product was frozen at −80°C post cell removal at the production site, and stored in 1 L bottles until further use. To adjust the sample volume, CCS from 1 L bottles has been thawed in a water bath at 25°C for 2–3 h, aliquoted into 50 ml centrifugation tubes by Corning Life Sciences at 45 ml and frozen at −80°C until further use. Before an experiment, the required number of aliquots have been thawed in a water bath at 25°C, pooled, and filtered with 0.2 µm filters. In total, the harvest was freeze-thawed twice and filtered once before conducting the case study. This may influence the outcome of the study, but mirrors typical handling of process development samples in industry. This said, the significant results obtained in this study highlight the mechanisms occurring in any FT process during sample handling. The twice freeze-thawed harvest before our study will be referred to as the "reference sample."

2.3 | FT process

Controlled freezing and thawing was done in a small-scale freezing device designed and manufactured in cooperation with Industrietechnik Salzburg Bilfinger. The freezing container is designed as a hollow tube cooled from the in- and outside. The used scale-down model is designed as a thin slice of a larger scale, that is separated into six wedges by an insulating inlay of polytetrafluoroethylene. A schematic drawing of the freezing device and a sample chamber is displayed in Figure 1.

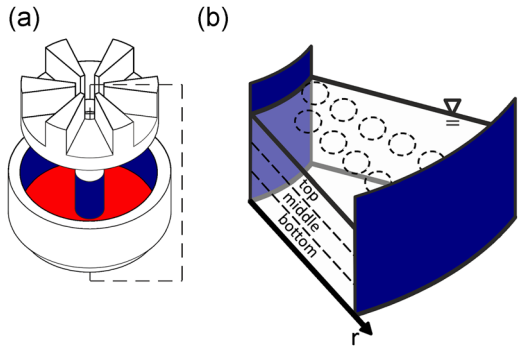

FIGURE 1 Freeze–thaw scale down model. (**a**) An exploded view of the device with two cooling walls in blue. The inlay is used to reduce boundary freezing from the bottom and for volume reduction. The bottom of the device is heated to further minimize freezing from the bottom. (**b**) A single chamber with sample layers and drill holes in the bulk volume as indicated by the dashed cross-section in (a). Images were adapted from Weber and Hubbuch (2021)

To reduce boundary conditions, an additional cooling circuit heats the wedge from the bottom at a constant temperature of 0°C. The detailed process and thermal process behavior are described thoroughly in a previous study on the characterization of freezing processes (Weber & Hubbuch, 2021).

All freezing experiments were performed in triplicates using three separated freezing chambers to account for process variation and assure reproducibility. Seventy-five milliliters of CCS prepared as described above was pipetted into each chamber. Then, the device was tempered at 5°C for at least 1 h for temperature equilibration throughout the system and the sample bulk. After temperature equilibration, freezing was initiated by lowering the cooling fluid temperature at maximum cooling rate to −60°C to −20°C. The final temperature was held for at least 5 h or overnight.

A core drill with 8 mm inner diameter from Buerkle was used for sampling from the frozen bulk. A 3D-printed lid was put on top of a chamber to assure reproducible sampling at three levels of 8 mm at nine locations with equal radial distances from each other as shown in Figure 1b. In preliminary experiments, radial freeze concentration was found negligible. Thus, samples were taken from two neighboring rows providing an increased number of overlapping samples volumes for improved data resolution. Afterwards, the frozen bulk was thawed by increasing the cooling fluid temperature to 25°C for 1.5 h before homogenization and final liquid sampling using a 5 ml pipette.

If a subsequent protein A capture step was performed, no frozen samples were taken. In this case, the device temperature was lowered to 5°C after thawing to reduce protein degradation while each replicate from a separate chamber was processed resulting in three separate protein A runs per freezing temperature. Therefore, samples were kept inside the cooled freezing device for up to 7 h at 5°C.

2.4 | mAb capturing

The mAb was captured from CCS using protein A affinity chromatography. MabSelect Sure was packed and operated with an ÄKTA-purifier system (Cytiva). UV extinction at 280 nm, pH, and conductivity were measured throughout the purification. An Omnifit column with 10 mm inner diameter from Omnifit Ltd. was used as column housing. The column was repacked throughout the experiments with column heights ranging from 188 to 203 mm resulting in a column volume (CV) of 14.7–15.9 ml. Sixty-five milliter samples with a titer of approximately 2–3 g/L mAb were loaded onto the column. As the manufacturer states a dynamic binding capacity of 35 g/ml resin, the column was operated well below its maximum capacity. The chromatography was conducted at a constant flow rate of 300 cm/h with PBS, pH 7.4 as equilibration and post-loading wash buffer. Twenty-five millimolar NaAc, pH 5 has been applied as a second wash followed by an elution with 25 mM acetic acid, pH 3 until 2 CV after the end of fraction collection. Product was collected in 15 ml fractions starting from an extinction of 0.2 AU until stopped below 0.1 AU. Fraction collection criteria were chosen based on recommendations by the harvest supplier. Detailed chromatography conditions are listed in the Supporting Information Material.

2.5 | Filtration analysis

In general, as some systems showed a high turbidity, 0.2 µm filtration was performed in between every FT and chromatography step to avoid clogging of the protein A capturing columns. A filtration cascade using syringe filters with 1.2, 0.45, and 0.2 µm cut-off from Sartorius was performed to investigate the size range of the particles present. The flow-through was analyzed for particles as described below.

Furthermore, the filter cake retained after a filtration step was investigated to measure the loss of mAb and host cell protein (HCP) through filtration post freezing and thawing. Therefore, Vivaspin 2 filters with a 0.2 µm cut-off polyethersulfone membrane from Sartorius were loaded with a sample volume V_{load} of 2–4 ml and centrifuged at 1200*g*. In preliminary experiments, 20 ml could be loaded onto the filter until filter clogging occurred. To reduce the influence of membrane fouling with increasing load volume, maximum load volumes of 4 ml were applied. After filtration, the filter membrane was detached from the housing, transferred into 500 µl centrifugation tubes and incubated with 500 µl $V_{dissolve}$ size-exclusion chromatography–high-performance liquid chromatography (SEC-HPLC) running buffer at 700 rpm and 5°C in a thermomixer comfort from Eppendorf overnight to dissolve any retained aggregates. As the filter membrane contained solution in the membrane pores after centrifugation, the measured protein concentration $c_{dissolve}$ in the dissolution buffer was composed of the dissolved filtered particles and the protein concentration from the filtered solution remaining in the filter. Thus, a mass balance over different load volumes V_{load} was used to calculate the aggregate concentration $c_{aggregate}$ in the

analyzed sample. The subtraction of mass balances with different load volumes eradicates the influence of the remaining solution in the pores and leads to the following equation:

$$c_{\text{aggregate}} = V_{\text{dissolve}} \frac{\Delta c_{\text{dissolve}}}{\Delta V_{\text{load}}} = V_{\text{dissolve}} m, \quad (1)$$

where m is the slope of a linear regression of $c_{\text{dissolved}}$ over V_{load}. Protein concentrations were determined by capillary electrophoresis, HPLC, and SEC as described below. As proteins tend to adsorb to the filter membrane, the flow-through was re-filtered in a separate experiment for comparison.

2.6 | Analytics

As this study aims to mimic typical process development conditions, analytics have been carefully chosen with respect to their application in industry. The most commonly used analytics involve enzyme-linked immunosorbent assay (ELISA) to quantify HCP (Wang et al., 2009), SEC for quantification of mAb monomers and aggregates and sodium dodecyl sulfate–polyacrylamide gel electrophoresis for protein size detection and quantification for low concentrated HCPs. While the analytics partially provide redundant data, comparability of redundant results is not always given due to lower limits of detection of the used methods. Additionally, the optical density of solutions can be correlated with the particle number of non-filtered samples. Statistical significance was analyzed using a paired-sample t test.

2.7 | HCP quantification

The automated CHO HCP ELISA Gyrolab Bioaffy 1000HC with Gyrolab CHO HCP Kit 1 by Gyros Protein Technologies AB has been used for HCP analysis. The assays have been performed according to the supplied manual with reagents and buffers from Gyros Protein Technologies AB. CCS and post-capture samples have been diluted 1:1000 and 1:10, respectively.

2.8 | Protein size analysis

Proteins have been classified and quantified using an automated denaturing capillary electrophoresis. The Protein Express Assay LabChip together with the Caliper LabChip GX II by PerkinElmer were operated according to the manual. All samples have been diluted 1:2 with ultrapure water (PURELAB Ultra) before denaturing conditions were induced by adding 24.5 µl of 1 M dithiothreitol (DTT) at 100°C for 5 min. For the analysis, proteins measured with approximately 30 and 60 kDa were regarded as light and heavy chains of the mAb, and the mAb concentration was calculated from the sum of the mentioned concentrations. It was further assumed that the detected HCPs did not possess a quaternary structure.

2.9 | Large particles analysis

The optical density was used as an indicator for large aggregates in non-filtered samples. Therefore, 400 µl of the sample was pipetted into a cuvette with 1 cm path length, and the extinction at 600 nm wavelength was measured in a photometer Infinite 200 by Tecan.

2.10 | mAb monomer and aggregate analysis

SEC-HPLC was performed using an mAb-specific TSKgel SuperSW mAb HTP column by Tosoh Bioscience with a 0.45 µm pre-column filter. The chromatography was performed on the HPLC UltiMate 3000 by Thermo Fisher Scientific equipped with a diode-array detector and a cooled auto-sampler. Each analysis was operated at 0.35 ml/min for 9.5 min with a running buffer consisting of 100 mM sodium phosphate, 250 mM NaCl at pH 7. Two hundered microliter samples were pipetted into a 0.45 µm filter plate, centrifuged into a microplate before covering with aluminum foil and placement into the cooled auto-sampler compartment, where 20 µl sample were injected onto the column for analysis. A baseline shift was observed when analyzing CCS. Therefore, CCS was spiked with concentrated post-capture material at different concentrations to evaluate accuracy of the assay. Furthermore, mAb aggregates have only been calculated, if SEC-HPLC led to a baseline separation of the peaks of interest. Besides the protein main absorption peak at 280 nm wavelength, the absorption ratio A260/A280 was used to evaluated the presence of DNA, which has an absorption peak at 260 nm.

2.11 | Protein concentration

The mAb concentration in post-capture samples was measured with Nanodrop 2000c by Thermo Fisher Scientific. Assuming a negligible HCP content, UV absorption was measured at 280 nm and protein concentration was calculated with an extinction coefficient of 1.5 $g \cdot L^{-1} \cdot cm^{-1}$.

3 | RESULTS

3.1 | mAb concentration from CCS using SEC-HPLC

The quantification of mAb monomer and dimer was done using SEC-HPLC in a manner similar to Paul et al. (2014). Spiking of the CCS with concentrated mAb was performed to validate the determination of mAb concentrations from absorption areas of SEC-HPLC chromatograms.

As shown in Figure 2a, the reference unspiked sample showed a monomer peak after 4.0 min and a dimer peak after 3.4 min retention time. Numerous individual HCPs eluted after the monomer peak

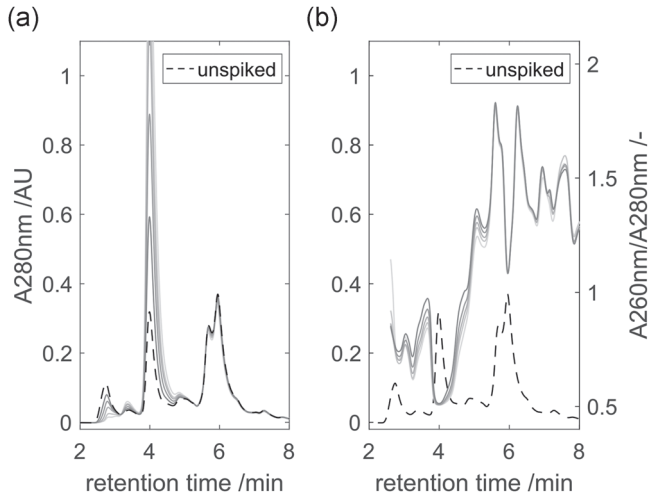

FIGURE 2 Size-exclusion chromatogram of cell culture supernatant spiked with concentrated monoclonal antibody. (**a**) Absorption at 280 nm (A280 nm) of spiked samples over retention time. The absorption is capped at 1.1 AU for visualization although monomer absorption exceeds the limit. (**b**) Absorption ratio calculated from absorption at 260 nm (A260 nm) divided by absorption at 280 nm. Data before 2.5 min retention time is not shown due to low signal-to-noise ratios. In both figures, the dashed line shows the absorption at 280 nm of the unspiked sample on the left *y* axis. Spike concentrations increase from dark to light from 1.8 to 10.0 g/L, respectively

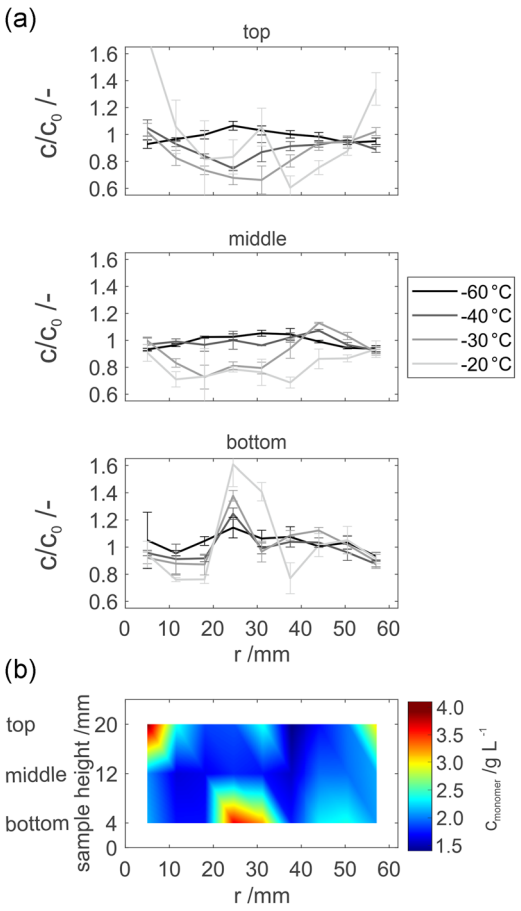

FIGURE 3 Concentration (*c*) profiles of monoclonal antibody (mAb) at different temperatures over the distance from the inner cooling wall (*r*). (**a**) Measured concentrations normalized by initial concentrations at the bottom, center, and top layers at 4, 12, and 20 mm above the bottom. The freezing temperatures rise with the gradient from dark to light from −60°C to −20°C. (**b**) mAb concentration of a cross-section as a contour map after freezing at −20°C. Data are interpolated in between measured samples and the whole bulk volume is displayed. Data extrapolation to the boundaries has been avoided

which could not be detected by SEC-HPLC in the protein A eluate (data not shown). The monomer and dimer absorption area at 280 nm increased with spike concentrations from 1.8 to 10.0 g/L. In contrast, the peak area after 2.7 min decreased with increasing spike concentration. Despite the fact that SEC-HPLC analysis did not lead to a baseline separation at the proteins of interest, a linear correlation between the monomer area and concentration was found with a coefficient of determination (R^2) of 0.9929 at a constant baseline at the global minimum. However, this correlation was only used for similar samples due to variances in the baseline shift that is expected to occur for varying contaminant concentrations. Figure 2b shows the absorption ratio A260/A280 of the samples. Data before 2.5 min retention time is not shown due to low signal-to-noise ratios. From 2.8 to 5.3 min retention time, the A260/A280 ratio decreases with increasing mAb concentration. For samples taken during elution of the mAb monomer from protein A, all ratios approach a minimum of 0.51. In comparison, a purified mAb sample approached a lower minimum A260/A280 ratio of 0.50.

3.2 | Freeze concentration profiles

The macroscopic freeze concentration in frozen bulks was investigated at freezing temperatures from −20 to −60°C. The mAb monomer concentrations c_{mab} relative to their initial concentration $c_{mab,0}$ are shown in Figure 3a over the cross-section of a freezing chamber at three individual layers. In Figure 3b, interpolated absolute concentrations are shown after freezing at −20°C.

In general, the bulk was more homogeneous with lower freezing temperatures and resulting freezing times. While relative concentrations (c/c_0) varied from 0.61- to 1.60-fold at a freezing temperature of −20°C, the concentrations after freezing at −60°C varied only from 0.91- to 1.06-fold. The highest concentration was found just left of the bottom center at all freezing temperatures, whereas the lowest concentration was found in the top layer for all experiments except when freezing at −60°C. The point of highest concentration matched the expected "last point to freeze" determined in a previous study (Weber & Hubbuch, 2021). The concentration differences from the bottom to top layer at $r = 25$ mm ($\Delta c = c_{b,25\,mm} - c_{t,25\,mm}$) from the inner cooling wall are 0.2, 1.1, 1.6, and 1.8 g/L at

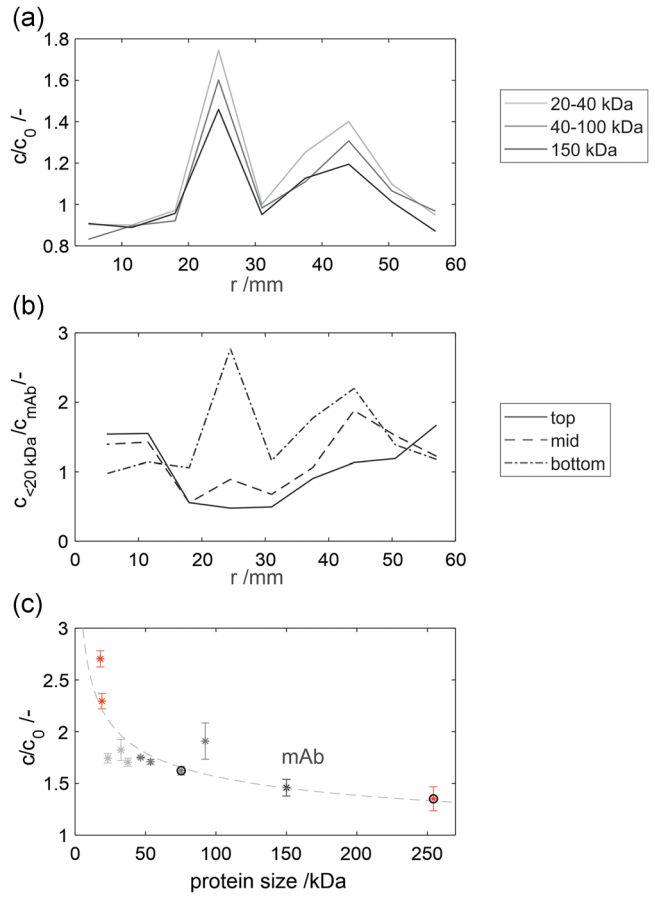

FIGURE 4 Protein size-dependent freeze concentration measured by capillary electrophoresis. (**a**) Mean protein concentrations (c) normalized by initial concentrations over the distance from the inner cooling wall (r) in the bottom layer. The harvest was frozen at −30°C in triplicates and proteins are grouped by size in kDa. (**b**) Freeze concentration of proteins smaller than 20 kDa normalized by the monoclonal antibody concentration in the three sample layers. (**c**) Freeze concentration at the point of highest concentration is plotted for all proteins over their respective sizes. If data points are circled, one outlier has been removed. Data were fitted to $y = (a/x^{\frac{1}{3}}) + b$. The color scheme in (**a**) and (**c**) is the same, and red data points in (**c**) are not shown in (**a**)

−60°C, −40°C, −30°C, and −20°C. When freezing at −60°C, the concentration increased toward the last point to freeze at $r = 25$ mm across all layers. At elevated freezing temperatures, however, the bulk concentration decreased toward the center in the top and middle layers. Higher freezing temperatures led to lower concentrations in the middle layer. In the top layer, a similar trend was found, except at the highest temperature of −20°C. Furthermore, with higher freezing temperatures, a local maximum in the bottom layer was found between the outer larger cooling wall and the global maximum. Finally, the average standard deviations from triplicates increase with freezing temperatures resulting in $\sigma_{-60°C} = 3.5\%$, $\sigma_{-40°C} = 3.5\%$, $\sigma_{-30°C} = 4.9\%$, and $\sigma_{-20°C} = 9.1\%$. The mean relative freeze concentration over all samples was calculated for each freezing temperature to show the accuracy of the method by a volume averaged mass balance. A closed mass balance would result in an average freeze concentration of 100%. Average freeze concentration decreased from 100 ± 5.5% to 96 ± 9.0% to 92 ± 15.6% to 94 ± 27.7% for freezing temperatures of −60°C, −40°C, −30°C, and −20°C, respectively.

3.3 | Protein size-dependent freeze concentration

In Figure 4a, freeze-concentrated proteins in the bottom layer after freezing at −30°C are depicted. A freezing temperature of −30°C was selected exemplarily as it led to a medium freeze concentration. The freeze concentration (c/c_0) of individual proteins has been measured by capillary electrophoresis. Freeze concentrations of up to 1.46 ± 0.08-fold for mAb were measured, which agrees with the measurements by SEC-HPLC reporting 1.38 ± 0.04-fold. For smaller HCP proteins, much higher freeze concentrations were detected such as 1.74- and 4.04-fold on average for proteins between 20 and 40 kDa and proteins smaller than 20 kDa, respectively. In the areas close to the cooling walls and at the local center minimum, the differences between the freeze concentration of small and large proteins were smaller. In the top layer right above the maximum freeze concentration, a relative mAb concentration of 35% was found in contrast to 52% for proteins between 20 and 40 kDa. When comparing the freeze concentration of small proteins to mAb as shown in Figure 4b, it was observed that small proteins show a high freeze concentration at the bottom and lower freeze concentration in the top layer. Thus, a separation of proteins as a function of size occurred. As shown in Figure 4c, the protein size correlates with the freeze concentration of the individual protein at bottom center with the highest concentration. Protein diffusivity increases with decreasing size and is thus suggested as a reason for the correlation. Under the assumption of spherical protein folding, the Einstein–Stokes equation can be used to calculate the diffusion coefficient D of spherical particles with radius R and volume V by $D = k_B T/6\pi\eta R$, where k_B is the Boltzmann constant, T the absolute temperature, and η is the viscosity. As the protein radius is proportional to the protein mass with $r \sim m^{1/3}$ (Torres et al., 2012), a data fit to $C/C_0 = (a/m^{\frac{1}{3}}) + b$ resulted in a root mean square error of 24.2% and R^2 of 0.634, where a and b are fitted parameters. The parameter a accounts for the constant parameters in the Einstein–Stokes equation and b is necessary because of the minimal freeze concentration of all solutes.

3.4 | Filtration analysis of thawed mAb CCS

After freezing and thawing of CCS, sometimes high turbidities can usually be observed visually. When thawed CCS was filtered using a filter cascade of decreasing pore size, the turbidity gradually decreased as shown in Table 1. The majority of the filtered particles (66%) was bigger in size than 1.2 µm, whereas 24.8% had a size

between 0.2 and 0.45 µm. Hence, 0.2 µm filtration before chromatography steps is necessary to avoid clogging of the columns. It has to be noted that several pre-syringe filters had to be used after freezing due to the large number of particles blocking the filter pores. This poses the question as to whether product is lost during filtration and critical quality attributes are changed. To analyze the particles filtered from a solution, a redissolution step of the retentate was performed. After a centrifugal filtration step, the membrane remains wet with soluble proteins in the retained solution. This leads to incorrect concentration measurements when incubating the filter membranes in redissolution buffer. Therefore, it is necessary to filter different filtration volumes, which is shown in Figure 5a, with exemplary raw data of replicates from individual freezing experiments.

Under the assumption of negligible membrane fouling, the redissolved protein concentration $c_{dissolve}$ should be proportional to the volume filtered V_{load}. Thus, a linear regression was performed for each experiment. This regression reduces measurement errors occurring due to standard deviations and membrane variation. Additionally, the concentration contribution of the solution retained in the membrane pores can be calculated from the *y* axis intercept.

TABLE 1 Turbidity reduction with filtration cascade

Filter pore size (µm)	Turbidity (mAu)	Turbidity reduction (mAu) (% of total)
Non-filtered	72.7 ± 0.75	n.a.
1.2	62.9 ± 0.25	9.8 (65.8%)
0.45	61.5	1.4 (9.4%)
0.2	57.8 ± 0.33	3.7 (24.8%)

When comparing the redissolved protein concentrations from CCS frozen at −40°C and −20°C, the regression slopes decrease from 11.7 to 1.9 $\mu g \cdot ml^{-1} \cdot ml^{-1}$ (µg protein per ml $V_{dissolve}$ and ml V_{load}) with statistical significance ($p = 0.04$). The particle concentrations calculated from the slopes are displayed in Figure 5b. More particles containing mAb and HCP are filtered on average when the solution is frozen at −20°C. While the concentration of the total protein content and the HCP in the particles could be reduced when lowering the freezing temperature to −40°C, the measured mAb concentration did not change significantly. Only a minor reduction in dimer shares when decreasing the freezing temperature was found on average. Adsorption of the proteins to the filter membrane did occur, but on average, it was always below the smallest concentration measured. The measured mAb concentration was approximately one order of magnitude lower than the concentration of HCP and total protein.

3.5 | Capturing of freeze-thawed mAb CCS

CCS from CHO was frozen at −40°C, −30°C, and −20°C to investigate the influence of freezing and thawing on critical quality attributes. As particles are formed post FT steps, filtration is necessary to avoid column clogging. When measuring the mAb aggregate and HCP content post FT and filtration, no significant changes were observed. HCP concentrations varied within 101 ± 6% and 117 ± 6% of the initial concentration without a trend regarding freezing temperature. The average initial HCP concentration was 1.45 g/L. The average mAb aggregate content post FT varied from 105 ± 2% to 97 ± 5% of the initial value. Although no significant difference was found, mAb aggregate shares post FT increased on

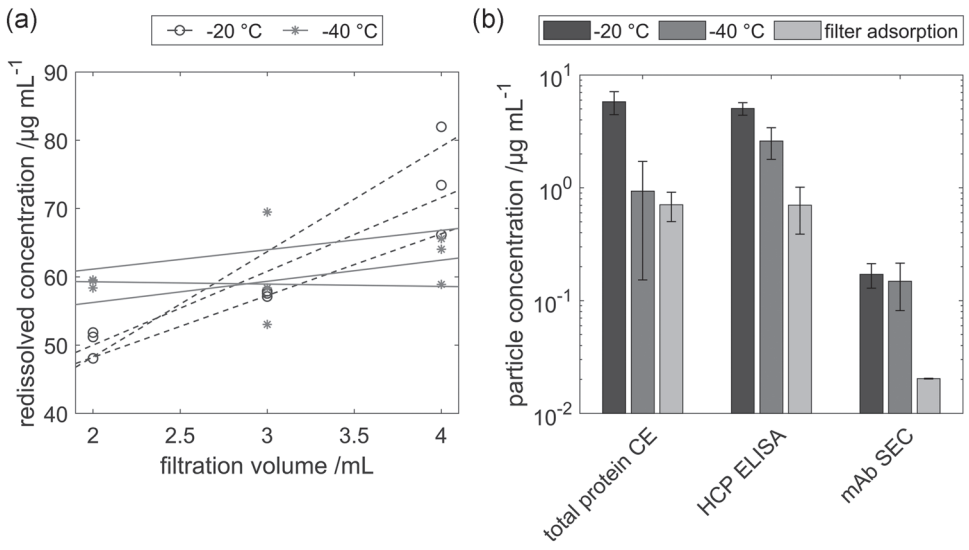

FIGURE 5 Retained proteins on a 0.2 µm filter. (**a**) Exemplary raw data from triplicates with their respective linear regressions. The total, redissolved protein concentration measured by capillary electrophoresis (CE) at −20 and −40°C is shown. Regression slopes from −40°C and −20°C in solid and dashed lines, respectively, are significantly different ($p = 0.04$) and used to calculate the initial particle concentration. (**b**) Particle concentrations of the total protein amount, host cell proteins (HCP), and monoclonal antibody (mAb). A log-scale *y* axis is shown. Protein adsorption to the filter is displayed for comparison

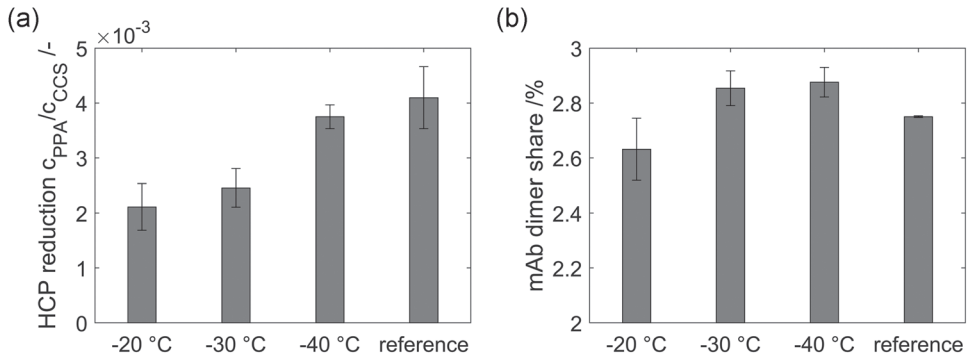

FIGURE 6 Analysis of post protein A (PPA) eluate. (**a**) Host cell protein (HCP) reduction after protein A. Concentrations (*c*) measured by enzyme-linked immunosorbent assay were normalized by the concentration in the cell culture supernatant (CCS). (**b**) The dimer share PPA measured by size-exclusion chromatography–high-performance liquid chromatography A280 area. Differences from −20°C to −40°C were significant in (a) for HCP recovery ($p = 0.04$) and in (b) for dimer shares ($p = 0.03$)

average with lower temperatures. However, the FT step and the applied freezing temperature affected the HCP and aggregate concentration in the protein A eluate as shown in Figure 6.

At lower freezing temperatures, the remaining HCP concentration was higher compared with the initial concentration. The remaining HCP concentration increased from 0.21 ± 0.04% to 0.37 ± 0.02% of the initial HCP concentration when lowering the temperature from −20°C to −40°C with significant difference ($p = 0.04$). In comparison, after capturing of mAb from the reference sample, almost twice as many HCPs (0.41 ± 0.06%) were found in the eluate. Likewise, the mAb aggregate content after freezing at −20°C and capturing was 2.63% and increased to 2.87% on average after freezing at −40°C with significant difference ($p = 0.03$). When compared with a reference mAb sample with aggregate shares of 2.75%, elevated freezing temperatures reduced the aggregate shares, whereas colder freezing temperatures lead to increased aggregate shares.

4 | DISCUSSION

4.1 | Correlation of mAb concentration to peak area

As shown in Figure 2, SEC-HPLC does not lead to baseline separation of the monomer and dimer peaks at 3.4 and 4.0 min, respectively. Analysis of a flow-through sample from a protein A load step with the majority of mAb removed revealed that a valley-to-valley baseline correction approaches the background noise of a CCS sample. Therefore, sample preparation before SEC-HPLC is often suggested (Dunn et al., 2020) to avoid co-elution of CCS contaminants. Alternatively, precise monomer and dimer quantification from crude CCS samples requires intense background correction of the spectra. In our case, a valley-to-valley baseline correction marginally improved our concentration prediction model from $R^2 = 0.9929–0.9934$, which is in the range of the analysis by Dunn et al. (2020) who reported an R^2 of 0.9961. However, this model can only be applied under similar background conditions and is expected to perform worse at low concentrations. Additionally, the absorption ratio A260/A280 reveals further model restrictions. As DNA has its absorption maximum at 260 nm, a decrease of the signal indicates either less DNA or a higher protein concentration. Generally, the A260/A280 ratio decreased with increasing spike concentrations except at the elution of the monomer. Therefore, we conclude that DNA in the CCS tends to stick to mAb monomers, which, in turn, may increase the apparent absorption at 280 nm with increasing mAb concentration. Due to the discussed model uncertainties, a baseline fixed to the global minimum to quantify monomer concentrations from CCS was found sufficient for the scope of this study. The analyzed samples share the same origin, and the background is expected to be similar. Unlike Paul et al. (2014), our spiking experiments suggest that the peak area at 2.7 min is not entirely mAb aggregates, as the area decreased with increasing spike concentrations. Additionally, the columns' void volume is expected to be around 1 ml, where the first peak elutes. Therefore, aggregate shares should not be as high as 75% in CCS as reported by Paul et al. (2014).

4.2 | Freeze concentration profile

Our finding of macroscopic freeze concentration for elevated freezing temperatures is a well-described phenomenon in slow freezing processes due to elevated temperatures or passive cooling (Hauptmann et al., 2019; Kolhe & Badkar, 2011; Reinsch et al., 2015). Freeze concentration of up to 160% agrees with findings by Webb et al. (2002), who reported a relative BSA concentration of 130% in a similar actively cooled setup. The concentration profile differences at low and high freezing temperatures can be explained by natural convection. As freezing temperatures are lowered, freeze front velocities increase resulting in faster freezing processes. Higher partition coefficients, that describe the entrapment of solute in the frozen matrix at the freezing front, have been reported at faster freezing

processes (Rodrigues et al., 2011) leading to reduced freeze concentration. Due to density gradients at the ice front, natural convection occurs causing high concentrations in the bottom layer (Rodrigues et al., 2013). Recent simulations by Geraldes et al. (2020) report velocities in the area of up to 1 mm/s when freezing at −10°C. Higher density gradients and slower freezing processes, therefore, promote an increased natural convection at high freezing temperatures. The CCS in this study contained different contaminants besides the mAb at 2 g/L such as media components and HCPs. These contaminants are also freeze-concentrated leading to a higher density gradient compared with an mAb solution at a similar concentration, such as final fill formulations. Under the assumption of comparable partition coefficients, natural convection will be more pronounced for denser bulk solutions. The increasing concentration toward the center across all layers at −60°C indicates a possible reduction of natural convection at such low freezing temperatures. However, with the occurrence of natural convection, effects such as second local concentration maximum and increased overall standard deviations appear. Fluctuation might occur with convection, which, in turn, leads to higher standard deviations. Furthermore, the convection is not only dependent on the physical properties of the solution, but also on the crystal morphology at the ice front, as the crystal structure is a stochastic effect. The observed top layer outlier close to the cooling walls at −20°C might be due to freeze concentrate pushed out of the center at the last point to freeze. After freezing was completed, the bulk surface showed a mountain-like shape. Therefore, samples above 22 mm height were discarded, except for the samples close to the cooling walls, where the bulk volume height did not exceed 22 mm. This was also described by Hauptmann et al. (2019). Increasing convection also led to larger inaccuracies of the sampling method. The mass balance did not close for the observed concentrations at elevated freezing temperatures.

4.3 | Natural convection amplifies solute separation by diffusion

Looking at the freeze concentration of differently sized proteins shown in Figure 4c, a correlation between freeze concentration and protein size can be found, where smaller proteins tend to freeze and concentrate more at the center bottom of a container. However, the relation between protein size and freeze concentration was only found when freeze concentration effects were high at the bottom of the freezing container. At points of lower freeze concentration at the bottom, the freeze concentration of different proteins was less significant. Fitting of the freeze concentration data at the point of highest concentration according to the correlation of diffusion to protein size, as shown in Figure 4c, revealed that protein diffusion might be an explanation. Besides diffusion, natural convection leads to an additional mass flux from the freeze-concentrated areas at the freezing front toward the center bottom, where size-dependent freeze concentration was most prominent. Natural convection is caused by density gradients due to freeze concentration and temperature differences leading to a convective layer in the gravitational direction at the freezing front (Rodrigues et al., 2011; Vynnycky & Kimura, 2007). The convection induces a circular motion, dragging down the solutes to the bottom and along the bottom of the freezing container in front of the freezing boundary, where it settles due to the higher density. Meanwhile, non-concentrated liquid from the center is transported to the freezing boundary, reducing the entrapped solute concentration and thus increasing inhomogeneity in the frozen bulk. On the one hand, natural convection is promoted by high concentration gradients leading to faster velocities at the freezing boundary. On the other hand, the convection at the freezing front is inhibited by crystallization such as dendritic ice formation (Miller et al., 2013). The density anomaly of water adds additional complexity to the mechanism. This complex behavior has been modeled (Geraldes et al., 2020; Ramesh et al., 2021) using the enthalpy-porosity method and the Carman–Kozeny equation to describe velocity through porous media (Kast et al., 2010). Figure 7 schematically depicts liquid fraction, temperature, velocity in gravitational direction, and concentration at the freezing front. Data are derived from numeric fluid simulation

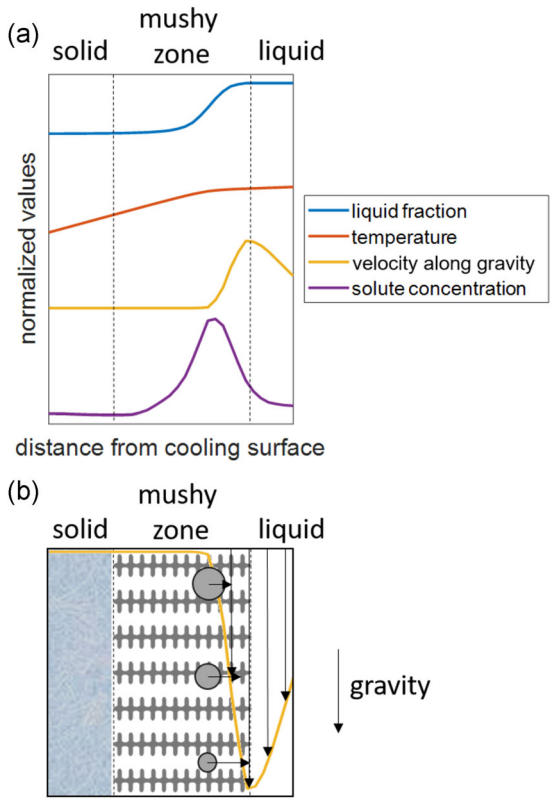

FIGURE 7 Schematic representation of mass transport at the freezing front. (**a**) Normalized values for liquid fraction, temperature, gravitational velocity, and solute concentration. Values originate from computational fluid dynamics simulation with enthalpy porosity method. (**b**) Schematic representation of the diffusion of three differently sized proteins shown as circles. The velocity profile of (**a**) in direction of gravity is shown and arrow length indicates the driving force

using velocity dumping method at the mushy zone according to a flow through porous media.

The convection velocity increases with solute concentration and liquid fraction, with the maximum velocity at the edge of the mushy zone. The solute concentration maximum is within the mushy zone, as the increasing velocity drags down the freeze-concentrated liquid and bring less concentrated liquid from the top and center. For detailed description of the mechanistic processes involved, the Grashof number and Prandtl number could be analyzed in further studies. Simulations show flow profiles thick as several millimeters at the beginning, which become thinner and slower over time (Geraldes et al., 2020). Smaller molecules with higher diffusivity might be able to diffuse further into the convective layer. Diffusive mass transport might be too slow for molecules to diffuse beyond the boundary layer. Hence, small proteins are exposed to faster drag velocities leading to a higher bottom freeze concentration. Experimental studies of flow profiles during solidification processes show the importance of such flow profiles (Shevchenko et al., 2015), which was also investigated by Geraldes et al. (2020), who simulated the effect of varying mushy zone porosities. Furthermore, the hypothesis is supported by an early study on freeze concentration, where buffer components were freeze-concentrated whereas the lactose dehydrogenase concentration was equal across the frozen bulk (Chen et al., 2001). Other studies have not found significant differences when comparing stabilizing formulation agents such as small buffer molecules and proteins like Roessl et al. (2014), who evaluated freeze concentration in an actively cooled small-scale model. The presumably low height of the container might have reduced natural convection and therefore minimized diffusion-based freeze concentration. The results by Kohle and Badkar (2011) show the mAb aggregate freeze concentration to be similar to that of the monomer, which can be explained by the minor variation in the diffusion coefficient, because of the relative large size of the proteins, which is above 150 kDa.

4.4 | FT of CCS leads to temperature-dependent formation of particles containing mAb and HCP

If the CCS was frozen, particles were formed during the FT step, that consist of both mAb and HCP as shown in Figure 6b. On average, all analytics show a reduction in particle formation with decreasing freezing temperature. As lower freezing temperatures lead to faster freezing processes, they induce less freeze stress and therefore reduce the rate of aggregation (Wöll et al., 2019). Furthermore, lower freezing temperatures lead to reduced freeze concentration as discussed before. Such particle formation might be induced by CHO HCPs such as protease cathepsin D (Bee et al., 2015) and thus, should be separated from the product as soon as possible. Furthermore, mAbs also form native aggregates under FT stress (Telikepalli et al., 2014).

The relatively low mAb concentration in the dissolution buffer can be explained by the presence of particles in the dissolution buffer. While ELISA and capillary electrophoresis are able to handle nonsoluble particles by dilution, wash steps or denaturation, HPLC methods require sample filtration and the use of a pre-column filter. Furthermore, ELISA and capillary electrophoresis are sensitive methods whereas the HPLC operates at the lower limit of the detection and is affected by model limitations as discussed earlier leading to relatively high standard deviations. Finally, capillary electrophoresis indicated a lower total protein concentration after −40°C FT than the measured HCP concentration.

Protein adsorption to filtration membranes is a common issue (Birk et al., 1995) and therefore has to be accounted for at such low concentration levels. The occurring membrane adsorption was lower than the measured particle concentration and thus can be interpreted as the background noise.

4.5 | Freezing influences critical quality attributes of mAb capturing

If CCS from CHO cells is frozen before capturing, significant changes in HCP and aggregate shares can be expected in the protein A eluate as depicted in Figure 6. HCP levels in the eluate are generally lower after a FT step followed by a necessary filtration compared with a reference sample. At first glance, the HCP concentration might be generally decreased by the particle removal, leading to an overall reduction of HCP in the protein A load and subsequently the eluate. However, the HCP content from an aliquot, after the FT step and after filtration did not change significantly. Thus, a hypothesis is suggested, where the changes in the protein A eluate may arise from specific HCPs with high mAb affinity due to protein interactions. Looking at mAb capturing processes, HCP co-elution with mAb from protein A occurs due to protein interactions between HCPs and the mAb–protein A complex (Bee et al., 2015; Nogal et al., 2012; Zhang et al., 2016). Hence, co-eluting HCPs show increased affinity toward mAbs. If FT stress is exerted on the CCS, the stress favors particle formation of these particular high-affinity HCPs and the mAb because of their affinity. As discussed earlier, warmer freezing temperatures exert stronger freeze stress causing increased particle formation. These particles contain small amounts of mAb and high-affinity HCPs that are removed before the protein A capturing. As a result, freezing and subsequent filtration of CCS decrease the HCP concentration in protein A eluate. Furthermore, the FT step induces mAb aggregation leading to higher aggregate shares (Telikepalli et al., 2014). As a result, slightly stressed and fast-frozen samples at −40°C show higher dimer shares compared with reference protein A eluate. However, the soluble dimer aggregates might form insoluble oligomers that are removed by a filtration step. As higher FT stress is applied at warmer freezing temperatures, larger particles are formed (Hauptmann et al., 2018), which might be caused by higher concentrations (Roefs & De Kruif, 1994). Hence, the protein A eluate from freezing steps with warmer freezing temperatures show reduced aggregate shares compared with faster frozen samples. Unfortunately, soluble dimer shares are determined by HPLC and thus,

mAb aggregate shares directly after FT steps cannot be determined without prior filtration.

5 | CONCLUSION

This study highlights the effect of freezing temperature with regard to particle formation of mAb CCS. Freezing reduced the number of HCPs present in the protein A eluate, which demonstrates the importance of the careful characterization of freezing processes in current platform process development. Furthermore, increased levels of mAb dimers with slower freezing processes were shown. Our results suggest particle formation of mAb and co-eluting HCPs with mAb affinity. In subsequent studies, the hypothesis of the co-eluting HCPs could further be examined by proteomics.

Furthermore, the study provides in-depth process understanding of freezing mechanisms involving complex multicomponent media. Solute diffusion in the mushy zone is suggested as an explanation of freeze concentration dependency on protein size. The complex interplay of diffusion and convection should be further evaluated in mechanistic studies, such as computational fluid dynamics, to improve the process understanding.

ACKNOWLEDGMENTS

The authors are grateful for the financial support by Bilfinger Industrietechnik Salzburg GmbH, Schwetzingen, Germany and for the material supply by Byondis Nijmegen, the Netherlands. Furthermore, the authors would like to thank Bas Kokke and Michel Eppink for proofreading of the manuscript. Open Access funding enabled and organized by Projekt DEAL.

CONFLICT OF INTERESTS

The authors declare that there are no conflict of interests.

DATA AVAILABILITY STATEMENT

The data that support the findings of this study are available from the corresponding author upon reasonable request.

ORCID

Dennis Weber https://orcid.org/0000-0002-8700-579X

REFERENCES

Authelin, J. R., Rodrigues, M. A., Tchessalov, S., Singh, S. K., McCoy, T., Wang, S., & Shalaev, E. (2020). Freezing of biologicals revisited: Scale, stability, excipients, and degradation stresses. *Journal of Pharmaceutical Sciences*, *109*(1), 44–61. https://doi.org/10.1016/j.xphs.2019.10.062

Baumann, P., & Hubbuch, J. (2017). Downstream process development strategies for effective bioprocesses: Trends, progress, and combinatorial approaches. *Engineering in Life Sciences*, *17*(11), 1142–1158. https://doi.org/10.1002/elsc.201600033

Bee, J. S., Tie, L., Johnson, D., Dimitrova, M. N., Jusino, K. C., & Afdahl, C. D. (2015). Trace levels of the CHO host cell protease cathepsin D caused particle formation in a monoclonal antibody product. *Biotechnology Progress*, *31*(5), 1360–1369. https://doi.org/10.1002/btpr.2150

Bhatnagar, B. S., Robin, H. B., & Michael, J. P. (2007). Protein stability during freezing: Separation of stresses and mechanisms of protein stabilization. *Pharmaceutical Development and Technology*, *12*(5), 505–523. https://doi.org/10.1080/10837450701481157

Birk, H.-W., Andrea Kistner, V. W., & Schütterle, G. (1995). Protein adsorption by artificial membrane materials under filtration conditions. *Artificial Organs*, *19*(5), 411–415. https://doi.org/10.1111/j.1525-1594.1995.tb02351.x

Butler, M. F. (2002). Freeze concentration of solutes at the ice/solution interface studied by optical interferometry. *Crystal Growth and Design*, *2*(6), 541–548. https://doi.org/10.1021/cg025591e

Chang, B. S., Brent, S. K., & John, F. C. (1996). Surface-induced denaturation of proteins during freezing and its inhibition by surfactants. *Journal of Pharmaceutical Sciences*, *85*(12), 1325–1330. https://doi.org/10.1021/js960080y

Chen, Y. H., Cao, E., & Cui, Z. F. (2001). An experimental study of freeze concentration in biological media. *Food and Bioproducts Processing*, *79*, 35–40.

Dunn, Z. D., Desai, J., Leme, G. M., Stoll, D. R., & Richardson, D. D. (2020). Rapid two-dimensional protein-A size exclusion chromatography of monoclonal antibodies for titer and aggregation measurements from harvested cell culture fluid samples. *mAbs*, *12*(1), 1702263. https://doi.org/10.1080/19420862.2019.1702263

Geraldes, V., Gomes, D. C., Rego, P., Fegley, D., & Rodrigues, M. A. (2020). A new perspective on scale-down strategies for freezing of biopharmaceutics by means of computational fluid dynamics. *Journal of Pharmaceutical Sciences*, *109*(6), 1978–1989. https://doi.org/10.1016/j.xphs.2020.02.012

Hauptmann, A., Georg Hoelzl, & Loerting, T. (2019). Distribution of protein content and number of aggregates in monoclonal antibody formulation after large-scale freezing. *AAPS PharmSciTech*, *20*(2), 1–11. https://doi.org/10.1208/s12249-018-1281-z

Hauptmann, A., Podgoršek, K., Kuzman, D., Srčič, S., Hoelzl, G., & Loerting, T. (2018). Impact of buffer, protein concentration and sucrose addition on the aggregation and particle formation during freezing and thawing. *Pharmaceutical Research*, *35*(5), 101. https://doi.org/10.1007/s11095-018-2378-5

Kast, W., Gaddis, E. S., Wirth, K.-E., & Stichlmair, J., (Revised by Hermann Nirschl). (2010). L1 pressure drop in single phase flow, e. V. VDI *VDI heat atlas* (2nd ed., pp. 1053–1116). Springer-Verlag. https://doi.org/10.1007/978-3-540-77877-6_70

Kolhe, P., & Badkar, A. (2011). Protein and solute distribution in drug substance containers during frozen storage and post-thawing: A tool to understand and define freezing-thawing parameters in biotechnology process development. *Biotechnology Progress*, *27*(2), 494–504. https://doi.org/10.1002/btpr.530

Mahler, H.-C., Friess, W., Grauschopf, U., & Kiese, S. (2009). Protein aggregation: Pathways, induction factors and analysis. *Journal of Pharmaceutical Sciences*, *98*(9), 2909–2934. https://doi.org/10.1002/jps.21566

Miller, M. A., Rodrigues, M. A., Glass, M. A., Singh, S. K., Johnston, K. P., & Maynar, J. A. (2013). Frozen-state storage stability of a monoclonal antibody: Aggregation is impacted by freezing rate and solute distribution. *International Journal of Pharmaceutical Sciences*, *102*(4), 1194–1208. https://doi.org/10.1002/jps

Nogal, B., Chhiba, K., & Emery, J. C. (2012). Select host cell proteins coelute with monoclonal antibodies in protein a chromatography. *Biotechnology Progress*, *28*(2), 454–458. https://doi.org/10.1002/btpr.1514

Paul, A. J., Schwab, K., & Hesse, F. (2014). Direct analysis of mAb aggregates in mammalian cell culture supernatant. *BMC Biotechnology*, *14*(1), 1–11. https://doi.org/10.1186/s12896-014-0099-3

Privalov, P. L. (1990). Cold denaturation of protein. *Critical Reviews in Biochemistry and Molecular Biology*, *25*(4), 281–306. https://doi.org/10.3109/10409239009090612

Ramesh, V., Terala, S., Mazumder, S., Matharu, G., Vaishnav, D., & Ali, S. (2021). Development and validation of a model for efficient simulation of freezing of water in large tanks. *Journal of Thermal Science and Engineering Applications*, *13*(1), 011008. https://doi.org/10.1115/1.4047166

Rayfield, W. J., Kandula, S., Khan, H., & Tugcu, N. (2017). Impact of freeze/thaw process on drug substance storage of therapeutics. *Journal of Pharmaceutical Sciences*, *106*(8), 1944–1951. https://doi.org/10.1016/j.xphs.2017.03.019

Reinsch, H., Spadiut, O., Heidingsfelder, J., & Herwig, C. (2015). Examining the freezing process of an intermediate bulk containing an industrially relevant protein. *Enzyme and Microbial Technology*, *71*, 13–19. https://doi.org/10.1016/j.enzmictec.2015.01.003

Rodrigues, M. A., Balzan, G., Rosa, M., Gomes, D., de Azevedo, E. G., Singh, S. K., Matos, H. A., & Geraldes, V. (2013). The importance of heat flow direction for reproducible and homogeneous freezing of bulk protein solutions. *Biotechnology Progress*, *29*(5), 1212–1221. https://doi.org/10.1002/btpr.1771

Rodrigues, M. A., Miller, M. A., Glass, M. A., Singh, S. K., & Johnston, K. P. (2011). Effect of freezing rate and dendritic ice formation on concentration profiles of proteins frozen in cylindrical vessels. *Journal of Pharmaceutical Sciences*, *100*(4), 1316–1329. https://doi.org/10.1002/jps

Roefs, S. P. F. M., & De Kruif, K. G. (1994). A model for the denaturation and aggregation of β-lactoglobulin. *European Journal of Biochemistry*, *226*(3), 883–889. https://doi.org/10.1111/j.1432-1033.1994.00883.x

Roessl, U., Jajcevic, D., Leitgeb, S., Khinast, J. G., & Nidetzky, B. (2014). Characterization of a laboratory-scale container for freezing protein solutions with detailed evaluation of a freezing process simulation. *Journal of Pharmaceutical Sciences*, *103*(2), 417–426. https://doi.org/10.1002/jps.23814

Shevchenko, N., Roshchupkina, O., Sokolova, O., & Eckert, S. (2015). The effect of natural and forced melt convection on dendritic solidification in Ga-In alloys. *Journal of Crystal Growth*, *417*, 1–8. https://doi.org/10.1016/j.jcrysgro.2014.11.043

Telikepalli, S. N., Kumru, O. S., Kalonia, C., Esfandiary, R., Joshi, S. B., Middaugh, C. R., & Volkin, D. B. (2014). Structural characterization of IgG1 mAb aggregates and particles generated under various stress conditions. *Journal of Pharmaceutical Sciences*, *103*(3), 796–809. https://doi.org/10.1002/jps.23839

Torres, J. F., Komiya, A., Okajima, J., & Shigenao, M. (2012). Measurement of the molecular mass dependence of the mass diffusion coefficient in protein aqueous solutions. *Defect and Diffusion Forum*, *326–328*, 452–458. https://doi.org/10.4028/www.scientific.net/DDF.326-328.452

Vynnycky, M., & Kimura, S. (2007). An analytical and numerical study of coupled transient natural convection and solidification in a rectangular enclosure. *International Journal of Heat and Mass Transfer*, *50*(25–26), 5204–5214. https://doi.org/10.1016/j.ijheatmasstransfer.2007.06.036

Wang, X., Hunter, A. K., & Mozier, N. M. (2009). Host cell proteins in biologics development: Identification, quantitation and risk assessment. *Biotechnology and Bioengineering*, *103*(3), 446–458. https://doi.org/10.1002/bit.22304

Webb, S. D., Webb, J. N., Hughes, T. G., Sesin, D. F., & Kincaid, A. C. (2002). Freezing bulk-scale biopharmaceuticals using common techniques—And the magnitude of freeze-concentration. *BioPharm*, *15*(5), 22–34.

Weber, D., & Hubbuch, J. (2021). Temperature based process characterization of pharmaceutical freeze-thaw operations. *Frontiers in Bioengineering and Biotechnology*, *9*, 1–9. https://doi.org/10.3389/fbioe.2021.617770

Wöll, A. K., Desombre, M., Enghauser, L., & Hubbuch, J. (2019). A phase diagram-based toolbox to assess the impact of freeze/thaw ramps on the phase behavior of proteins. *Bioprocess and Biosystems Engineering*, *43*, 179–192. https://doi.org/10.1007/s00449-019-02215-5

Zhang, Q., Goetze, A. M., Cui, H., Wylie, J., Tillotson, B., Hewig, A., Hall, M. P., & Flynn, G. C. (2016). Characterization of the co-elution of host cell proteins with monoclonal antibodies during protein A purification. *Biotechnology Progress*, *32*(3), 708–717. https://doi.org/10.1002/btpr.2272

SUPPORTING INFORMATION

Additional Supporting Information may be found online in the supporting information tab for this article.

How to cite this article: Weber, D., Sittig, C., & Hubbuch, J. (2021). Impact of freeze–thaw processes on monoclonal antibody platform process development. *Biotechnology and Bioengineering*, 118, 3914–3925. https://doi.org/10.1002/bit.27867